Journal of Magnetism and Magnetic Materials 595 (2024) 171933

Contents lists available at ScienceDirect

Journal of Magnetism and Magnetic Materials

journal homepage: www.elsevier.com/locate/jmmm

Research article

Magnetic phase tuning in patronite-based VS_4 nanowires

Renato B. Moreira [a], Leandro Seixas [a,b,*]

[a] School of Engineering, Mackenzie Presbyterian University, Rua da Consolação, 930, São Paulo SP. 01302-907, Brazil
[b] MackGraphe — Mackenzie Institute for Research in Graphene and Nanotechnologies, Mackenzie Presbyterian Institute, Rua da Consolação, 896, São Paulo SP. 01302-907, Brazil

ARTICLE INFO

Keywords:
Patronite
VS4
Nanowires
Phase transition
Magnetic semiconductor

ABSTRACT

Magnetic semiconductors have the potential to push the boundaries of emerging technologies like spintronics. They could change the way we process and store data by leveraging not just the electron charges, but also their intrinsic spin. Materials with low dimensionality, specifically one- or two-dimensional materials, are key to this advancement. Within this category, one-dimensional semiconductors with either antiferromagnetic or ferromagnetic properties are particularly interesting for their electronic and magnetic properties. However, creating and maintaining stable ferromagnetic ordering in these semiconductors is not straightforward. There are significant challenges, such as issues due to the disorder of dopants in dilute magnetic semiconductors, or stability problems in two-dimensional magnetic materials like chromium triiodide (CrI_3). In this work, we show a potential solution in VS_4 nanowires, a one-dimensional material found in patronite minerals. These nanowires can have four magnetic orderings: two antiferromagnetic (AFM1 and AFM2), one ferrimagnetic (FI), and one ferromagnetic (FM) ordering, which we can access using different strains. We observe two magnetic phase transitions with strains in the plastic (non-linear) regime. The nanowire transitions from AFM1 to AFM2 with ϵ_z = 6.8 %, and from AFM2 to FM with ϵ_z = 11.8 %. This ability to tune the magnetic phases in a semiconductor material opens up a vast range of opportunities for their integration into spintronic devices. We believe that the range of magnetic phases in a one-dimensional semiconductor, like VS_4 nanowires, could lead to the enhanced control of both charge and spin in nanotechnology devices.

1. Introduction

The discovery of graphene established a novel research direction in which nanomaterials were defined by their van der Waals (vdW) interactions [1–4]. Lamellar materials bonded by vdW interactions were the main sources of discoveries related to these novel low-dimensional materials. Since the vdW interactions in these materials are weaker than the covalent and ionic bonds, in many cases, it is possible to exfoliate these lamellar materials down to a single layer. In addition to the exfoliation of lamellar materials, two-dimensional (2D) materials can also be synthesized using a bottom-up approach, such as crystal growth by chemical vapor deposition [5] or molecular-beam epitaxy methods [6]. Minerals have also been important to the discovery and design of novel 2D lamellar materials. The natural occurrence of these minerals guarantees the stability and raw material needed for the exfoliation of the materials. For example, molybdenum disulfide (MoS_2) is naturally found in molybdenite minerals [7], and the 2D topological insulator Pt_2HgSe_3 can be obtained from the mineral jacutingaite [8,9]. Additionally, there are examples of mineral-based 2D materials for clinochlore [10] and phyllosilicates [11].

Patronite is a mineral formed by VS_4 nanowires bonded through vdW interactions. It was discovered in 1906 in Cerro de Pasco, Peru. However, it was only in 1964 that it was characterized by Allman et al. [12] The crystal is formed by centers of V^{4+} bonded by moieties of $(S_2^{2-})_2$, as shown in Fig. 1(a). Nanowires interact with each other weakly via the van der Waals force. The crystal has a $C2/c$ space group, a monoclinic crystal system, and the following experimental lattice parameters: a = 12.11 Å, b = 10.42 Å, c = 6.78 Å, and β = 100.8°. VS_4 is a semiconductor material with an optical band gap of 1.35 eV [13].

VS_4 materials have been synthesized for applications in energy storage devices, such as supercapacitors and cathode materials for lithium–sulfur batteries [14–17]. These batteries have been noteworthy for their very high energy densities (2600 Wh kg^{-1}), high specific capacities (1675 mAh g^{-1}), and their use of abundant, cost-effective sulfur cathodes. A persistent issue, however, arises from the formation of lithium polysulfides (LiPS), which exhibit high solubility in the electrolyte and can diffuse to the anodes, drastically reducing the battery's lifespan [18]. Polar sulfur compounds, such as VS_4, have been recently incorporated into sulfur cathodes and can anchor the

* Corresponding author at: School of Engineering, Mackenzie Presbyterian University, Rua da Consolação, 930, São Paulo SP. 01302-907, Brazil.
E-mail address: leandro.seixas@mackenzie.br (L. Seixas).

https://doi.org/10.1016/j.jmmm.2024.171933
Received 12 September 2023; Received in revised form 24 January 2024; Accepted 7 March 2024
0304-8853/© 2024 Elsevier B.V. All rights reserved.

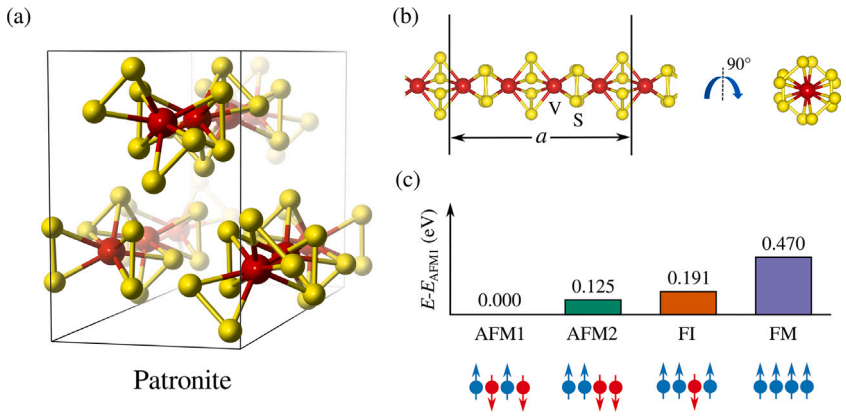

Fig. 1. (a) A schematic representation of the patronite crystal structure (bulk), with VS_4 nanowires bonded by the van der Waals force. (b) A schematic representation of an isolated VS_4 nanowire. Lateral (left panel) and cross-section (right panel) views of the VS_4. (c) The total energy difference with relation to the AFM1 ordering (in eV). The ordering of the magnetic moments is shown below the energy diagram.

LiPS and increase the battery charge and discharge efficiency. For a long time, the controlled synthesis of VS_4 was quite challenging. There are challenges associated with keeping the stoichiometry fixed and not synthesizing VS_2 or other vanadium sulfides. Today, synthetic VS_4 with well-defined stoichiometry is grown on graphic substrates, such as doped carbon nanotubes or graphene oxide [13,15,16].

It is interesting to note that the magnetic properties of VS_4 can be interesting for other applications, such as nanoelectronic, magnetic, and optical devices. Intrinsic VS_4 nanowires are antiferromagnetic semiconductors, with V^{4+} ions with local magnetic moments of $m = 1.17\ \mu_B$ and antiparallel alignments [19]. The d orbitals of the V^{4+} ions interact with neighboring V^{4+} ions through the p orbitals of the S. This indirect interaction causes coupling between the d orbitals, known as a superexchange, and stabilizes the antiferromagnetic ordering.

Magnetic semiconductors are of great interest in spintronics, particularly for devices such as spin-field-effect transistors and magnetic memories. In the quest for magnetic semiconductors, some materials have been created by doping non-magnetic semiconductors with transition metals, forming diluted magnetic semiconductors [20]. However, the disorder of semiconductor dopants has created great challenges for controlling magnetic semiconductors. Therefore, intrinsic magnetic semiconductors are very interesting, especially when external factors can be used to handle the magnetic ordering.

A couple of years ago, Li et al. [19] studied the electronic and magnetic properties of VS_4 nanowires through *ab initio* simulations. While the intrinsic VS_4 nanowire is an antiferromagnetic semiconductor, doping the material with electrons or holes makes it a half-metal antiferromagnetic material (HMAF) [19]. This material only conducts through a single spin state. HMAF materials are interesting for creating completely spin-polarized electrical currents. There are small variations in the local magnetic moments with charge transfer, but the coupling between the local magnetic moments has been antiparallel aligned for all studied dopings. They showed that the Néel temperature for the antiferromagnetic semiconductor was $T_N = 210$ K [19], well above those of other materials such as CrI_3 bilayers ($T_N = 45$ K) [21]. For higher temperatures, other magnetic orderings can be observed in this material. At room temperature, it was observed through ^{51}V nuclear magnetic resonance (NMR) measurements that the patronite-based VS_4 is a diamagnetic material, even in the presence of magnetic dipoles of the V^{+4} ions [22].

For spintronic devices, the ferromagnetic and antiferromagnetic ordering of materials is important. Ferromagnetic materials are important for creating memories that use the effect of giant magnetoresistance and also for spin torque transistors [23]. Antiferromagnetic materials are also being investigated for antiferromagnetic spintronics. Zero total magnetization with alternating local magnetic moments is an interesting prospect for creating devices that do not suffer from interference from magnetic fields or the external magnetization of nearby components [24,25]. Thus, semiconductor materials with tunable magnetic phases can be of great interest in developing disruptor spintronic devices.

In this article, we investigate the electronic, mechanical, and magnetic properties of VS_4 nanowires with four different magnetic orderings (two distinct antiferromagnetic, a ferrimagnetic, and a ferromagnetic order). These phases are investigated by applying strains in the elastic and plastic regimes. We study the fundamental properties of VS_4 that can contribute to developing nanoelectronic and spintronics devices. In addition, a qualitative analysis of the ligand effects of VS_4 on the AFM1 ordering is presented, which helps explain the magnetic phase transition.

2. Materials and methods

Our first-principles simulations were carried out using the density functional theory (DFT) [26,27] implemented in the Siesta code [28]. We utilized norm-conserved Troullier–Martins pseudopotentials [29] and a mesh cutoff of 400 Ry. The atomic orbitals were established on a double-ζ polarized (DZP) basis set, with an energy shift of 0.03 eV used for the confinement of the basis. The exchange–correlation functional used was the PBEsol approximation, a revision of the Perdew–Burke–Ernzerhof (PBE) [30] exchange–correlation functional more appropriate for solids [31]. We sampled the Brillouin zone with the Monkhorst–Pack algorithm using nine k-points in the z-direction [32]. All geometries were optimized with forces smaller than 0.01 eV $Å^{-1}$. We used vacuum spacing of at least 15 Å in x and y directions to avoid interactions between periodic images. For the projected density of states (PDOS) calculations, we used a fine grid with 100 k-points in the Brillouin zone and a Gaussian smearing of $\sigma = 0.05$ eV. The analysis of bonds between orbitals was performed using the crystal orbital Hamilton population (COHP) method [33,34]. For the simulations of bulk materials, we used exchange–correlation functionals with a non-local correction of the van der Waals forces, such as the VV10 functional [35]. A sampling of k-points for the bulk was performed with a Monkhorst–Pack grid of dimensions $5 \times 5 \times 5$. The exfoliation energy was calculated by comparing the energy of a fictitious two-dimensional film of VS_4 nanowires with the bulk and using the surface area of this film [36]. All computational simulations were performed at a temperature of 0 K.

3. Results and discussion

Before delving into the features of the nanowires, determining their capability to be exfoliate from bulk materials can provide some insight.

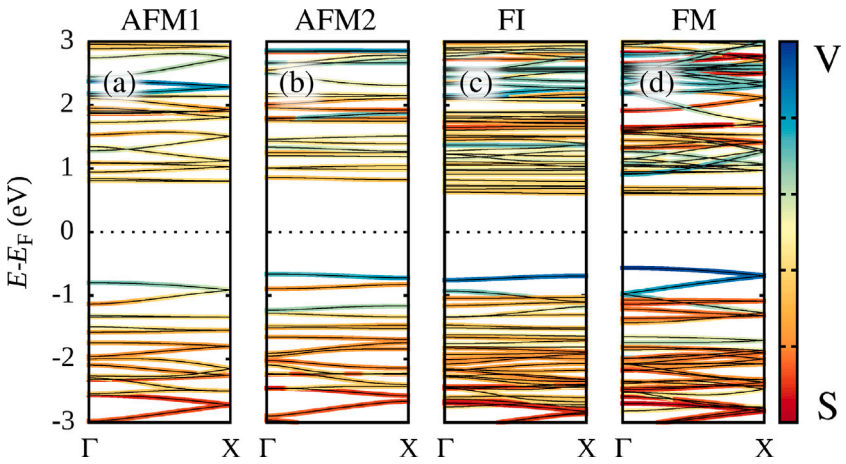

Fig. 2. The orbital-resolved electronic band structures of VS_4 for different magnetic orderings: (a) AFM1, (b) AFM2, (c) FI, (d) FM. Bloch states with higher projections onto vanadium orbitals are shown in blue, while those with higher projections onto sulfur orbitals are shown in red.

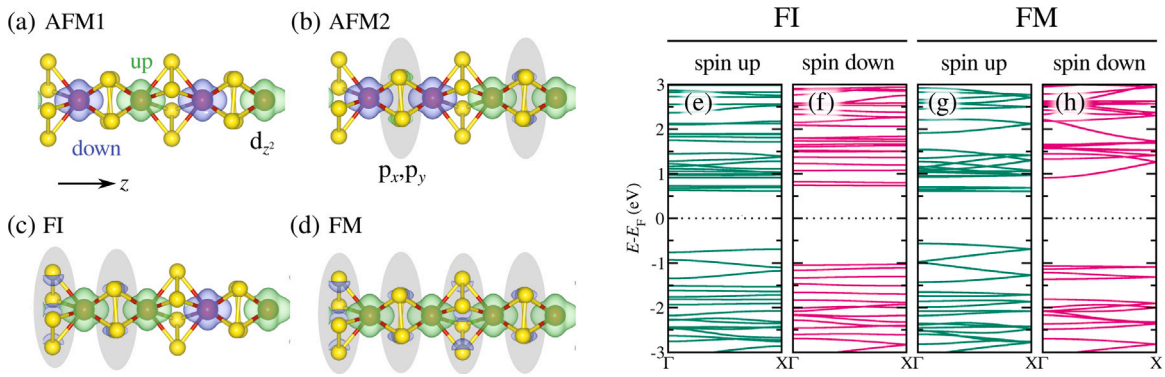

Fig. 3. Spin densities for the (a) AFM1, (b) AFM2, (c) FI, and (d) FM orderings. The isosurfaces were calculated with a spin density constant of $\rho_s = \pm 0.05\ e/a_0^3$. Green (blue) surfaces represent positive (negative) spin densities. Spin-resolved electronic band structures of VS_4: (e,f) FI and (f,g) FM. Spin-up (-down) bands are shown in green (pink).

Table 1
The lattice constants (a), electronic band gaps (E_g), and net magnetic moments per unit cell (m) for the four magnetic orderings.

Magnetic ordering	a (Å)	E_g (eV)	m (μ_B)
AFM1	12.295	1.60	0.0
AFM2	12.392	1.49	0.0
FI	12.434	1.31	2.0
FM	12.618	1.17	4.0

We estimated the energy required for exfoliation using the combined energies of the bulk and a fictitious two-dimensional VS_4 film. We found the exfoliation energy to be $\gamma = 14.2$ meV Å^{-2}. Employing the Mounet criterion [36], we inferred that VS_4 can be classified as an easily-exfoliated material since $\gamma < 35$ meV Å^{-2}. In these computational models, exchange–correlation functionals with a van der Waals force correction are applied to both the bulk and two-dimensional VS_4 film. The easy exfoliation of VS_4 agrees with the experimental results for forming colloidal dispersions with sonified VS_4 in organic solvents [37].

We isolated a single nanowire from the bulk VS_4, as shown in Fig. 1(b). The optimized lattice constant of VS_4 depends on the magnetic ordering of the V^{4+} ions. We investigated nanowires with four different magnetic orderings: single antiferromagnetic (AFM1), double antiferromagnetic (AFM2), ferrimagnetic (FI), and ferromagnetic (FM). The orientations of the magnetic moments of these magnetic orderings are shown in Fig. 1(c), as well as the differences between the total energies and lowest energy state (AFM1). It is important to note the difference between the AFM1 and AFM2 orderings. In the AFM1 ordering, the magnetic moments of the V^{4+} ions alternate for each neighboring ion. Meanwhile, in the AFM2 ordering, the alternating magnetic moments are grouped every two V^{4+} ions. The FI ordering is defined by the imbalance between magnetic moments with up and down spins. There is a net magnetization of $m_{FI} = 2.0\ \mu_B$ per unit cell. For the FM ordering, all ions of V^{4+} have their magnetic moments aligned in the same direction. The net magnetization for this ordering is $m_{FM} = 4.0\ \mu_B$ per unit cell. We observed that the lowest energy state was that of AFM1, followed by AFM2, FI, and FM, as shown in Fig. 1(c). The VS_4 lattice constants for these magnetic orderings are shown in Table 1. Note that the lattice constant of the FM ordering is 2.6% higher than that of the AFM1 ordering.

3.1. Electronic band structures

The electronic band structures of VS_4 were analyzed with projections of the V and S atomic orbitals, as shown in Fig. 2. The color map illustrates projections onto atomic orbitals. Bloch states that have significant contributions from vanadium orbitals are represented in blue, whereas those that primarily consist of contributions from sulfur orbitals are depicted in red. The bands for VS_4 with the magnetic orderings AFM1, AFM2, FI, and FM indicate that the material is a semiconductor in all cases investigated, with some variations in the bandgap sizes and valence band dispersions. The bandgaps calculated at the PBEsol level are shown in Table 1. Note that there is a difference of 0.43 eV between the bandgaps of the magnetic orders AFM1 and FM. For the FI ordering, the bandgap is direct, with a conduction

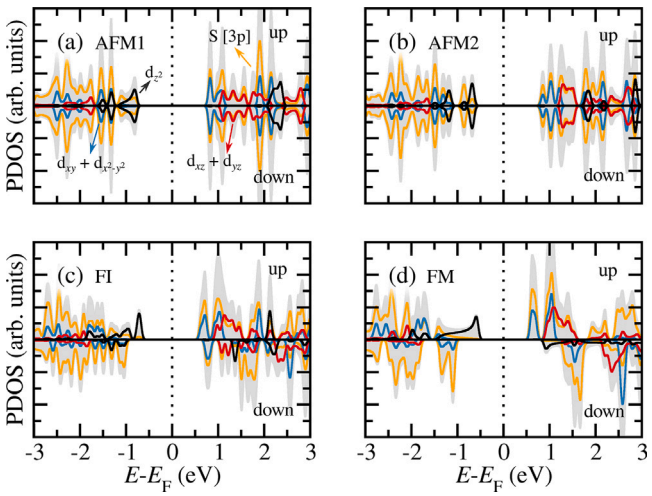

Fig. 4. Projected density of states (PDOS) for (a) AFM1, (b) AFM2, (c) FI, (d) FM. S[3p] orbitals are plotted in orange, V[d_{z^2}] in black, V[d_{xz}+d_{yz}] in red, and V[d_{xy}+$d_{x^2-y^2}$] in blue. The total density of states (DOS) is represented by the shaded gray area.

band minimum (CBM) and a valence band maximum (VBM) at the X-point. However, the bandgap is indirect for orderings AFM1, AFM2, and FM. The CBM is at the X-point, and the VBM is at the Γ-point. We can also observe that the conduction band mostly comprises sulfur p orbitals, while the valence band comprises vanadium d orbitals. Thus, the selection rules allow first-order optical transitions between the first empty conduction band and the last-filled valence band. In addition, based on simulations of the VS_4 bulk at the PBEsol level and lattice parameters with van der Waals corrections, we found a band gap of 1.22 eV. This PBEsol band gap is very close to the experimental band gap (E_g^{exp} = 1.35 eV) [13].

From the spins-up ($\rho_\uparrow$) and spin-down ($\rho_\downarrow$) charge densities, we can calculate the spin density ($\rho_s = \rho_\uparrow - \rho_\downarrow$). The isosurfaces for the spin densities for each magnetic ordering are shown in Fig. 3(a). When two V^{4+} cations have the same spin orientation, the anions $(S_2^{2-})_2$ have opposite orientations to the cations, with the spin densities highlighted in gray. However, this opposite spin density in the anions $(S_2^{2-})_2$ does not change the net magnetization, which is $m_{FI} = 2\ \mu_B$ per unit cell in the FI ordering, and $m_{FM} = 4\ \mu_B$ per unit cell in the FM ordering. We also did not observe opposite spin densities in the anions between cations with alternating spin, as found in the AFM1, AFM2, and FI cases.

For the VS_4 bands in the FI and FM orders, there is a difference between spin-up and spin-down electronic states. Therefore, in Fig. 3, we show the bands of these magnetic orderings with the separation of the spin degrees of freedom (spin-resolved electronic band structure). In the FI ordering, the bands of the electronic spin-up states are shown in Fig. 3(b), and those of the spin-down states are shown in Fig. 3(c). For the FM ordering, the bands for the spin-up and spin-down electronic states are depicted in Fig. 3(d) and (e). We can see that both the conduction band minimum and the valence band maximum are spin-up polarized. The edges of the bands with spin-down polarization are at energies farther from the Fermi level. Individually analyzing the bands of the states separated by spin polarization, we see that there is a variation in the bandgaps, with $E_g^{\uparrow}(FI) = 1.31$ eV and $E_g^{\downarrow}(FI) = 1.77$ eV for the FI ordering, and $E_g^{\uparrow}(FM) = 1.17$ eV and $E_g^{\downarrow}(FM) = 1.99$ eV for the FM ordering. The valence bands for the spin-up states also show greater dispersion, while the valence bands for spin-down states are more localized. The spin-down states of the FM ordering show a greater dispersion for the conduction bands, while the spin-up states for the FI and FM orderings and the spin-down states for the FI ordering are quite localized.

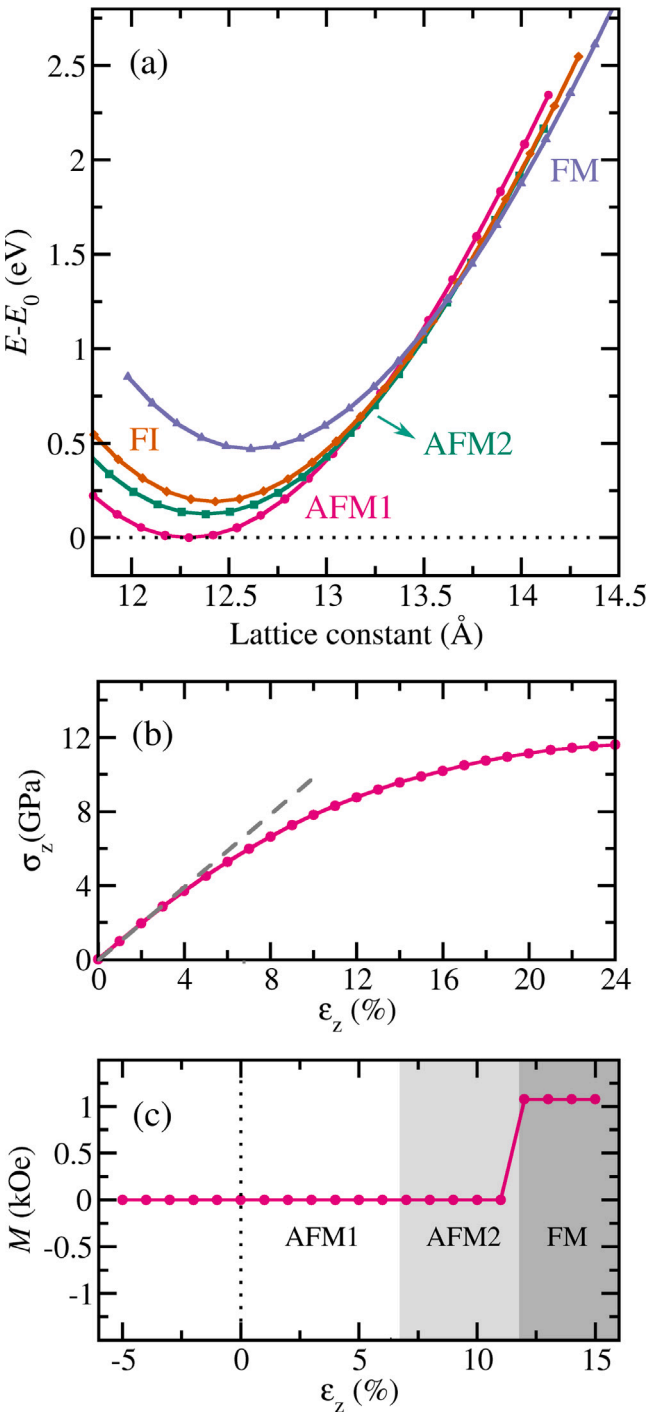

Fig. 5. (a) The strain-induced magnetic phase transition of VS_4. (b) The engineering stress–strain curve for a VS_4 nanowire. The linear elastic approximation is shown by the gray dashed line. (c) The evolution of the magnetization with strains in the z direction. Strains above $\varepsilon_z = 6.8\%$ induce a phase transition from AFM1 to AFM2, and strains above $\varepsilon_z = 11.8\%$ induce ferromagnetic ordering.

3.2. Projected density of states

The projected densities of states (PDOS) were calculated for nanowires with magnetic orderings AFM1, AFM2, FI, and FM. Due to orbital hybridization, we separated the electronic states by the p orbitals of sulfur, S[3p], and three groups of d orbitals of vanadium atoms, V[d_{z^2}], V[d_{xy}+$d_{x^2-y^2}$], and V[d_{xz}+d_{yz}]. Due to the nanowire symmetry, the d_{xy} orbitals were grouped with the $d_{x^2-y^2}$ orbitals,

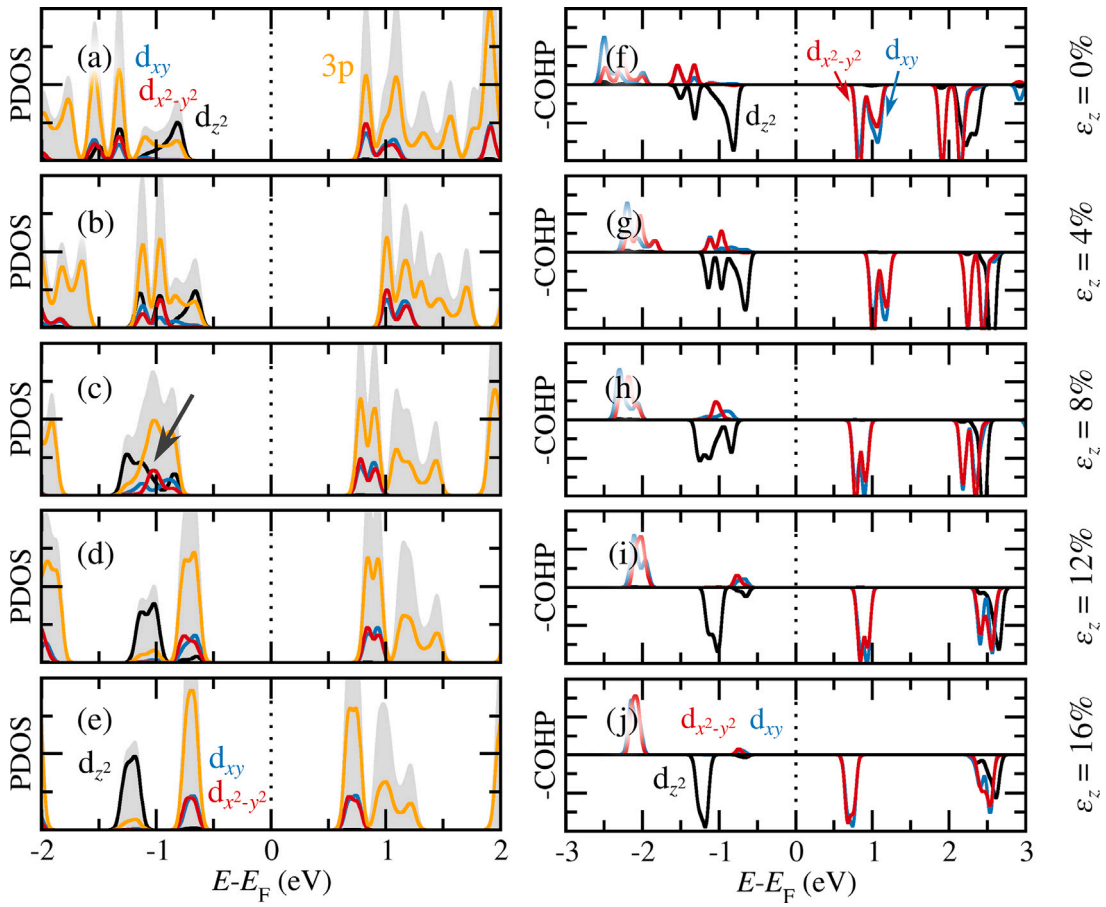

Fig. 6. The evolution of the electronic properties of VS_4 with AFM1 ordering and strains in the z direction. The projected density of states (PDOS) with strains in the z direction: (a) $\varepsilon_z = 0\%$, (b) $\varepsilon_z = 4\%$, (c) $\varepsilon_z = 8\%$, (d) $\varepsilon_z = 12\%$, (e) $\varepsilon_z = 16\%$. The total densities of states (DOS) are represented by a shaded area in gray. All DOS are shown in arbitrary units. The crystal orbital Hamilton population (COHP) with strains in the z direction calculated for V–V neighbors are: (f) $\varepsilon_z = 0\%$, (g) $\varepsilon_z = 4\%$, (h) $\varepsilon_z = 8\%$, (i) $\varepsilon_z = 12\%$, (j) $\varepsilon_z = 16\%$. The bonding (antibonding) orbitals are indicated by positive (negative) values of –COHP.

making the PDOS for each of these orbitals practically equal. Using the same justification, we grouped the d_{xz} orbitals with the d_{yz} orbitals. We also separated the orbitals of the spin-up and spin-down states, as shown in Fig. 4. For the magnetic orderings AFM1 and AFM2, the PDOS of the spin-up states is identical to that of the spin-down states. However, for the FI and FM orderings, these PDOS are quite different. In all cases, the top of the valence band is mostly V[d_{z^2}] orbitals and S[3p] orbitals, while the bottom of the conduction band is formed by V[d_{xy}+$d_{x^2-y^2}$] states and S[3p] orbitals.

3.3. Magnetic phase transition

Given that different magnetic orderings correspond to different lattice constants, we expected that by altering these lattice constants with strains, we could observe transitions in the magnetic orderings. Consequently, we computed how the total energy of the magnetic states would change when subjected to strains ranging from high compression (−5%) to high tension (+15%). For the purposes of our investigation, we varied the applied strains to pinpoint regions where magnetic transitions occurred. Fig. 5(a) illustrates the total energy for each magnetic ordering in relation to the lattice constant. The AFM1 ordering has the lowest energy with a lattice constant of a = 12.295 Å. In the absence of any applied strain, this state serves as our reference energy (E_0) for energy variations. We note that for lattice constants around 13.3 Å, the AFM2 ordering becomes the lowest energy. This magnetic transition occurs for strains around ε_z = 6.8%. For more significant strains, there is another magnetic phase transition, from AFM2 to FM, at strains around ε_z = 11.8%. Although this is also a high value for a strain, it is still close to that obtained experimentally for nanowires. High strain values like these are obtained experimentally in silver [38] and ZnO [39] nanowires. By using the double tangent method to determine the magnetic phase transitions when stress was applied, we found that the first magnetic transition (from AFM1 to AFM2) was expected to occur at around 5.4 GPa. On the other hand, the second magnetic transition (from AFM2 to FM) was expected to occur when the stress level reached 7.3 GPa. These stresses (< 14 GPa) are within the experimental capability of nanowires [39]. From the derivative of the elastic energy (the variation of the total energy with strain), we calculated the stress σ_z and obtained the strain–stress relation, as shown in Fig. 5(b). For this study, we calculated the elastic energy variation up to $\varepsilon_z = 24\%$ for the AFM1 ordering. The calculated Young's modulus is E = 98.4 GPa, with the linear tangent shown by the gray dashed line in Fig. 5(b). The elastic regime is defined by the 0.2% offset yield strength that intersects the curve at ε_{yield} = 3.75%. Thus, for strains greater than 3.75%, the deformation is plastic. Both the AFM1 → AFM2 and AFM2 → FM transitions occur in the plastic regime. The plasticity of deformations for phase transitions can be used for phase stabilization. Releasing material with plastic deformations tends to help partially maintain a residual deformation, which can stabilize the FM ordering.

The total (net) magnetization of the nanowires as a function of the strain is shown in Fig. 5(c). We notice that between strains from −5% (compressive) to +6.8% (tensile), the total magnetization is null due to the balance between the alternating magnetic moments of the V^{4+} cations of the AFM1 ordering. For strains greater than 6.8%, the total magnetization remains zero, although the magnetic ordering is different. There is still an equilibrium of magnetic moments in the

AFM2 ordering. For strains greater than 11.8%, there is a step in total magnetization to approximately $M = 1.07$ kOe ($\mu_0 M = 0.107$ T). Note that the FI ordering does not have the lowest energy for any strain value studied in this work.

3.4. Bonding and antibonding orbitals

To qualitatively understand why the magnetic phase transition occurs, we calculate the electronic properties of VS_4 nanowires with AFM1 ordering by applying strains. In Fig. 6(a)–(e), we show the evolution of the projected density of states (PDOS) as a function of strain: (a) 0%, (b) 4%, (c) 8%, (d) 12%, (e) 16%. As the spin-up and spin-down states have the same PDOS in AFM1 ordering, only a single spin state is shown. In the figure, the PDOS curves for the p orbitals of sulfur are shown in yellow, the PDOS curves for the $d_{x^2-y^2}$ orbitals in red, the d_{xy} orbitals in blue, and the d_{z^2} orbitals in black. The gray shaded area shows the total density of states.

From examining the PDOS as a function of the strain, we observe that the d_{z^2} states in the valence band are shifted to lower energies for larger strains. Meanwhile, the $d_{x^2-y^2}$ and d_{xy} states in the valence band, initially at lower energies than the d_{z^2} states, are shifted to higher energies with the application of strains. The crossing of these states that are decreasing in energy with those that are increasing in energy is shown in Fig. 6(c), around 1 eV below the Fermi level (highlighted by the gray arrow). This effect occurs due to the effective hopping of d_{z^2} orbitals with other d_{z^2} orbitals of neighboring vanadium atoms. By increasing the spacing between atoms, the effective hopping decreases, causing the bonding orbitals to approach the antibonding orbitals. During this process, the energies of the bonding orbitals increase while the energies of the antibonding orbitals decrease. When the state crossing occurs, around 8%, the wave function at the top of the valence band changes symmetry. This change destabilizes the AFM1 ordering for strains greater than 8%, favoring AFM2 or FM ordering.

The bonding, antibonding and nonbonding characteristics of crystalline orbitals can also be analyzed using the crystal orbital Hamilton population (COHP), which quantitatively evaluates the bond between chosen atomic orbitals. We examined the bonding between d_{z^2}-d_{z^2}, d_{xy}-d_{xy}, and $d_{x^2-y^2}$-$d_{x^2-y^2}$ orbital pairs between neighboring vanadium atoms. As the absolute value of the COHP indicates antibonding orbitals for positive values, bonding orbitals for negative values, and nonbonding orbitals for null values, we evaluated the magnitude of –COHP as a function of energy. The results are shown in Fig. 6(f)–(j) for strains: (f) 0%, (g) 4%, (h) 8%, (i) 12%, (j) 16%. We can see that the antibonding characteristics of the d_{z^2} orbitals agree with the previous analysis of the energy shifts of the PDOS peaks with strain. The bonding characteristics of the d_{xy} and $d_{x^2-y^2}$ orbitals also agree with the PDOS analysis. When applying strains, the bonding and antibonding orbitals shift in opposite directions. However, we note that the COHP peak intensity for d_{xy} and $d_{x^2-y^2}$ orbitals decreases significantly, indicating the formation of nonbonding orbitals. Still considering the small COHP values, we can observe an effective bonding characteristics for the 12% and 16% strains. Finally, this qualitative analysis of the crystalline bonds indicates a possible instability of the AFM1 ordering with high strains. In fact, magnetic phase transitions occur from strains of 6.8%, according to the change in symmetry of the wave function at the top of the valence band.

4. Conclusion

VS_4 nanowires are semiconductors possessing a broad range of magnetic phases, which can be finely tuned through the application of strains. Without any strain, this material is an antiferromagnetic semiconductor exhibiting local alternating magnetic moments (AFM1). When subjected to specific strains, the material undergoes a phase transition to a different antiferromagnetic ordering in which local magnetic moments alternate every two V^{4+} ions (AFM2). Further increasing the strain leads to another magnetic phase transition, where the AFM2-ordered material shifts into a ferromagnetic state (FM). This transformation creates a step-like increase in the total magnetization of the material as a function of the applied strain. The strains required to induce these phase transitions fall into the plastic regime, reaching up to 11.8% for stabilizing the FM ordering. While these levels of plastic deformation might appear large, they are comparable to those applied to other one-dimensional materials as reported in the scientific literature. We have managed to qualitatively understand these magnetic phase transitions through changes in the symmetry of the wave function at the valence band edge. This ability to control a broad spectrum of magnetic phases within VS_4 nanowires, simply by applying strain, suggests promising potential for applications in spintronic devices. Such applications range from magnetic memory storage systems to spin-field-effect transistors.

CRediT authorship contribution statement

Renato B. Moreira: Formal analysis, Methodology, Validation, Visualization. **Leandro Seixas:** Conceptualization, Funding acquisition, Methodology, Project administration, Software, Supervision, Visualization, Writing – original draft, Writing – review & editing.

Declaration of competing interest

The authors declare that they have no known competing financial interests or personal relationships that could have appeared to influence the work reported in this paper.

Data availability

Data will be made available on request.

Acknowledgments

The authors acknowledge financial support from the Fundo Mackenzie de Pesquisa e Inovação (MackPesquisa), Brazil (Grant No. 221018), Coordenação de Aperfeiçoamento de Pessoal de Nível Superior (CAPES), Brazil, Conselho Nacional de Desenvolvimento Científico e Tecnológico (CNPq), Brazil (Grant No. 311324/2020-7), INCT Materials Informatics, Brazil (Grant No. 406447/2022-5), and Fundação de Amparo a Pesquisa do Estado de São Paulo (FAPESP), Brazil (Grant No. 2022/14549-3). We also thank the High Performance Computing Center (NACAD) at COPPE, UFRJ for providing computational facilities.

References

[1] K.S. Novoselov, A.K. Geim, S.V. Morozov, D. Jiang, Y. Zhang, S.V. Dubonos, I.V. Grigorieva, A.A. Firsov, Electric field effect in atomically thin carbon films, Science 306 (2004) 666.
[2] S. Manzeli, D. Ovchinnikov, D. Pasquier, O.V. Yazyev, A. Kis, 2D transition metal dichalcogenides, Nat. Rev. Mater. 2 (2017) 17033.
[3] K.S. Novoselov, D. Jiang, F. Schedin, T. Booth, V. Khotkevich, S. Morozov, A.K. Geim, Two-dimensional atomic crystals, Proc. Natl. Acad. Sci. USA 102 (2005) 10451.
[4] J.N. Coleman, M. Lotya, A. O'Neill, S.D. Bergin, P.J. King, U. Khan, K. Young, A. Gaucher, S. De, R.J. Smith, et al., Two-dimensional nanosheets produced by liquid exfoliation of layered materials, Science 331 (2011) 568.
[5] J. Zhang, F. Wang, V.B. Shenoy, M. Tang, J. Lou, Towards controlled synthesis of 2D crystals by chemical vapor deposition (CVD), Mater. Today 40 (2020) 132.
[6] J. Dong, L. Zhang, X. Dai, F. Ding, The epitaxy of 2D materials growth, Nature Commun. 11 (2020) 5862.
[7] H. Shalchian, J.V. Khaki, A. Babakhani, G. Taglieri, I. De Michelis, V. Daniele, F. Veglio, On the mechanism of molybdenite exfoliation during mechanical milling, Ceram. Int. 43 (2017) 12957.
[8] A. Marrazzo, M. Gibertini, D. Campi, N. Mounet, N. Marzari, Prediction of a large-gap and switchable Kane-Mele quantum spin hall insulator, Phys. Rev. Lett. 120 (2018) 117701.

[9] R. Longuinhos, A. Vymazalová, A.R. Cabral, S.S. Alexandre, R.W. Nunes, J. Ribeiro-Soares, Raman spectrum of layered jacutingaite (Pt_2HgSe_3) crystals—experimental and theoretical study, J. Raman Spectrosc. 51 (2020) 357.
[10] R. de Oliveira, L.A. Guallichico, E. Policarpo, A.R. Cadore, R.O. Freitas, F.M. da Silva, V. d. C. Teixeira, R.M. Paniago, H. Chacham, M.J. Matos, et al., High throughput investigation of an emergent and naturally abundant 2D material: Clinochlore, Appl. Surf. Sci. 599 (2022) 153959.
[11] R. de Oliveira, A.R. Cadore, R.O. Freitas, I.D. Barcelos, Review on infrared nanospectroscopy of natural 2D phyllosilicates, J. Opt. Soc. Am. A 40 (2023) C157.
[12] R. Allmann, I. Baumann, A. Kutoglu, H. Rösch, E. Hellner, Die kristallstruktur des patronits $V(S_2)_2$, Naturwissenschaften 51 (1964) 263.
[13] C.S. Rout, B.-H. Kim, X. Xu, J. Yang, H.Y. Jeong, D. Odkhuu, N. Park, J. Cho, H.S. Shin, Synthesis and characterization of patronite form of vanadium sulfide on graphitic layer, J. Am. Chem. Soc. 135 (2013) 8720.
[14] E. Flores, E. Muñoz-Cortés, J. Bodega, O. Caballero-Calero, M. Martín-González, C. Sánchez, J.R. Ares, I.J. Ferrer, Beyond mono-, di-, and trisulfides: Synthesizing vanadium tetrasulfide (VS_4) films for energy conversion, ACS Appl. Energy Mater. 1 (2018) 2333.
[15] S. Wang, H. Chen, J. Liao, Q. Sun, F. Zhao, J. Luo, X. Lin, X. Niu, M. Wu, R. Li, et al., Efficient trapping and catalytic conversion of polysulfides by VS_4 nanosites for Li–S batteries, ACS Energy Lett. 4 (2019) 755.
[16] L. Luo, J. Li, H. Yaghoobnejad Asl, A. Manthiram, In-situ assembled VS_4 as a polysulfide mediator for high-loading lithium–sulfur batteries, ACS Energy Lett. 5 (2020) 1177.
[17] H. MP, A. Chandra Bose, Recent advances and future perspectives of VS_4 and its nanostructure composites for supercapacitor applications: A review, Energy Fuels 37 (2023) 10799.
[18] A. Manthiram, Y. Fu, Y.-S. Su, Challenges and prospects of lithium–sulfur batteries, Acc. Chem. Res. 46 (2013) 1125.
[19] S. Li, J. He, P. Nachtigall, L. Grajciar, F. Brivio, Doping isolated one-dimensional antiferromagnetic semiconductor vanadium tetrasulfide (VS_4) nanowires with carriers induces half-metallicity, J. Mater. Chem. C 9 (2021) 3122.
[20] K. Sato, L. Bergqvist, J. Kudrnovskỳ, P.H. Dederichs, O. Eriksson, I. Turek, B. Sanyal, G. Bouzerar, H. Katayama-Yoshida, V. Dinh, T. Fukushima, H. Kizaki, R. Zeller, First-principles theory of dilute magnetic semiconductors, Rev. Modern Phys. 82 (2010) 1633.
[21] B. Huang, G. Clark, D.R. Klein, D. MacNeill, E. Navarro-Moratalla, K.L. Seyler, N. Wilson, M.A. McGuire, D.H. Cobden, D. Xiao, et al., Electrical control of 2D magnetism in bilayer CrI_3, Nat. Nanotechnol. 13 (2018) 544.
[22] S. Britto, M. Leskes, X. Hua, C.-A. Hébert, H.S. Shin, S. Clarke, O. Borkiewicz, K.W. Chapman, R. Seshadri, J. Cho, et al., Multiple redox modes in the reversible lithiation of high-capacity, Peierls-distorted vanadium sulfide, J. Am. Chem. Soc. 137 (2015) 8499.
[23] I. Žutić, J. Fabian, S.D. Sarma, Spintronics: Fundamentals and applications, Rev. Modern Phys. 76 (2004) 323.
[24] T. Jungwirth, X. Marti, P. Wadley, J. Wunderlich, Antiferromagnetic spintronics, Nat. Nanotechnol. 11 (2016) 231.
[25] V. Baltz, A. Manchon, M. Tsoi, T. Moriyama, T. Ono, Y. Tserkovnyak, Antiferromagnetic spintronics, Rev. Modern Phys. 90 (2018) 015005.
[26] P. Hohenberg, W. Kohn, Inhomogeneous electron gas, Phys. Rev. 136 (1964) B864.
[27] W. Kohn, L.J. Sham, Self-consistent equations including exchange and correlation effects, Phys. Rev. 140 (1965) A1133.
[28] A. García, N. Papior, A. Akhtar, E. Artacho, V. Blum, E. Bosoni, P. Brandimarte, M. Brandbyge, J. Cerdá, F. Corsetti, et al., Siesta: Recent developments and applications, J. Chem. Phys. 152 (2020) 204108.
[29] N. Troullier, J.L. Martins, Efficient pseudopotentials for plane-wave calculations, Phys. Rev. B 43 (1991) 1993.
[30] J.P. Perdew, K. Burke, M. Ernzerhof, Generalized gradient approximation made simple, Phys. Rev. Lett. 77 (1996) 3865.
[31] J.P. Perdew, A. Ruzsinszky, G.I. Csonka, O.A. Vydrov, G.E. Scuseria, L.A. Constantin, X. Zhou, K. Burke, Restoring the density-gradient expansion for exchange in solids and surfaces, Phys. Rev. Lett. 100 (2008) 136406.
[32] H.J. Monkhorst, J.D. Pack, Special points for Brillouin-zone integrations, Phys. Rev. B 13 (1976) 5188.
[33] R. Dronskowski, P.E. Blöchl, Crystal orbital Hamilton populations (COHP): Energy-resolved visualization of chemical bonding in solids based on density-functional calculations, J. Phys. Chem. 97 (1993) 8617.
[34] S. Steinberg, R. Dronskowski, The crystal orbital hamilton population (COHP) method as a tool to visualize and analyze chemical bonding in intermetallic compounds, Crystals 8 (2018) 225.
[35] O. Vydrov, T. Van Voorhis, Nonlocal van der Waals density functional: The simpler the better, J. Chem. Phys. 133 (2010) 244103.
[36] N. Mounet, M. Gibertini, P. Schwaller, D. Campi, A. Merkys, A. Marrazzo, T. Sohier, I.E. Castelli, A. Cepellotti, G. Pizzi, et al., Two-dimensional materials from high-throughput computational exfoliation of experimentally known compounds, Nat. Nanotechnol. 13 (2018) 246.
[37] M.N. Kozlova, Y.V. Mironov, E.D. Grayfer, A.I. Smolentsev, V.I. Zaikovskii, N.A. Nebogatikova, T.Y. Podlipskaya, V.E. Fedorov, Synthesis, crystal structure, and colloidal dispersions of vanadium tetrasulfide (VS_4), Chem. Eur. J. 21 (2015) 4639.
[38] R. Ramachandramoorthy, W. Gao, R. Bernal, H. Espinosa, High strain rate tensile testing of silver nanowires: Rate-dependent brittle-to-ductile transition, Nano Lett. 16 (2016) 255.
[39] B. Wei, K. Zheng, Y. Ji, Y. Zhang, Z. Zhang, X. Han, title size-dependent bandgap modulation of ZnO nanowires by tensile strain, Nano Lett. 12 (2012) 4595.